Large-Eddy Simulation of Film Cooling

Xuyao GUO, Wolfgang SCHRÖDER, Matthias MEINKE

Aerodynamisches Institut, RWTH Aachen
Wüllnerstr. zw. 5 u 7, 52062 Aachen, Germany
Tel: +49-241-8095410, Fax: +49-241-8092257, E-mail: office@aia.rwth-aachen.de

ABSTRACT

The flow field induced by the interaction between a single jet flow exhausting from a pipe and a turbulent flat plate boundary layer at a local Reynolds number of $Re_\infty = 400,000$ is numerically studied using large-eddy simulation (LES). The ratio R of the jet velocity to the cross stream velocity is 0.1. The flow regime investigated corresponds to that of gas turbine blade film cooling. In order to provide the realistic time-dependent turbulent inflow information for the crossflow an LES of a spatially developing turbulent boundary layer is simultaneously performed using a rescaling method for compressible flow. The numerical method used to solve the governing equations is validated by comparing the solution of a turbulent boundary layer simulation with data from the literature. The main flow features such as the recirculation area downstream of the jet exit and the counter-rotating vortex pair (CVP) formed in the far field, which have a significant influence on the cooling efficiency, are analyzed.

NOMENCLATURE

$C_{1,2,3}$	coefficients in temperature rescaling
c	local sound velocity
c_p	specific heat
e	energy
D	diameter of jet hole
F, f	flux
H	difference of inviscid fluxes and viscous fluxes, thickness of flat plate
J	metric Jacobian
k	conductivity
L	reference length
$\overline{\overline{M}}$	symmetric matrix
Ma	Mach number
n	normal-wall direction
Pr	Prandtl number
p	pressure
Q	vector of conservative variables
q	Fourier's heat flux
R	ratio of jet velocity to crossflow velocity
Re	Reynolds number
r	recovery factor
S	spanwise distance between holes, additional source terms in sponge layer
$\overline{\overline{S}}$	symmetric part of velocity gradient tensor decomposition
T	temperature
t	time
U	contravariant velocities, streamwise velocity averaged in spanwise direction and in time
u, v, w	velocity components in Cartesian frame
u_τ	friction velocity
x, y, z	Cartesian coordinate directions
y^+	wall coordinate
α_l	Runge-Kutta coefficients
Γ	fine scale energy flux
γ	specific heat ratio c_p/c_v
δ	boundary layer thickness
θ	momentum thickness
λ_2	criterion for vortex identification
μ	molecular viscosity
ν	kinetic viscosity
ξ	generalized frame of reference
ρ	density
σ	Stokes tensor, factor used in source terms
τ	fine scale stress
χ	factor used in AUSM scheme
ψ	rescaling factor
$\overline{\overline{\Omega}}$	asymmetric part of velocity gradient tensor decomposition

Indices

a	analytical solution
c	convective term in AUSM scheme
I	inviscid flux
in	inlet position
$inner$	inner region of boundary layer
$outer$	outer region of boundary layer
p	pressure term in AUSM scheme
re	rescaling position
V	viscous flux
x, y, z	partial derivatives with respect to x, y, z
α	direction of generalized frame of reference
β	direction of Cartesian frame
0	inlet
$\pm$	left and right side of cell surface
∞	free-flow quantity

-   grid-filtered quantity
/   fluctuation of quantity

If not otherwise mentioned Einstein's summation convention is used for double indices.

INTRODUCTION

The rise in overall performance of gas turbines by a high inlet temperature poses quite a challenge to the material of the blade surface. Despite the noticeable progress made in blade metallurgy, a reasonable lifetime of turbine blades can be only ensured by an efficient surface cooling mechanism such as film cooling. This technique offers an excellent compromise between surface protection and aerodynamic efficiency, since unlike convective blade cooling it minimizes the thermal loads on other components of the turbine.

In film cooling the coolant is introduced to the hot gas stream of the turbine section through small holes drilled in the surface of the blades. The coolant forms a film layer over the blade surface to protect the surface from direct exposure to the hot gas stream. Due to the interaction between the coolant jet and the surrounding laminar or turbulent boundary layer around the blade the flow in the vicinity of the discharge holes is particularly complex. The cooling efficiency is influenced by many parameters (Gartshore et al., 2001) such as the injection angle, the geometry of the hole, the blowing ratio R of the jet velocity to the cross stream velocity, to mention just a few.

Over the last two decades a large amount of research has been carried out to understand the physics of the process and to improve the film cooling efficiency (Chernobrovkin and Lakshminarayana, 1999). The numerical simulation of such problems requires a correct prediction of the interaction between the cooling jet and the cross flow, which is characterized by the development of horseshoe-like and kidney vortices formed upstream and downstream of the jet exit. Up until very recently, the only feasible means of numerically simulating such a flow has been through solving the Reynolds-averaged Navier-Stokes equations using algebraic (Bohn et al., 1997) or two-equation turbulence models (Garg and Ameri, 1997). These turbulence models, however, usually fail to predict accurately vortex dominated flow fields. The results underpredict the lateral spreading rate of the jet and overpredict the penetration of the jet into the boundary layer. Since the vortex structures, the penetration depth of the cooling jet into the boundary layer and the recirculation area formed on the leeside of the jet exit have a significant influence on the film cooling mechanism, it is necessary to apply a more general method to analyze the interaction of the jet flow with the crossflow.

It is known in the literature that large-eddy simulation (LES) is a powerful concept for turbulent flow problems with strong streamline curvature, separated and swirling flow areas, and vortex shedding. Increasing experience of how to apply LES and the steady improvement in computer performance brought more and more flows of industrial interest within the range of analysis via LES. To investigate in more detail the flow field and the vortex dynamics in the vicinity and further downstream of the jet exit an LES method is used in this study.

The paper is organized as follows. After a brief description about the governing equations and the numerical method used to solve these equations, the flow model and the boundary conditions are presented. To verify the numerical method a turbulent boundary layer over a flat plate is simulated first. The streamwise velocity profiles and the turbulence intensities are compared with analytical solutions and data from the literature, respectively. Finally, the turbulent flow field of the jet in a crossflow is numerically analyzed and discussed at length.

GOVERNING EQUATIONS

The governing equations for an LES are obtained by a convolution of the Navier-Stokes equations for an ideal gas with a low-pass filter of width Δ, which corresponds in this study to a local average in each grid cell (Rogallo and Moin, 1984). The filtered equations read in a generalized frame of reference $\xi_\alpha = \xi_\alpha(x_\beta)$ ($\beta = 1, 2, 3$ and $\alpha = 1, 2, 3$)

$$J\frac{\partial \bar{Q}}{\partial t} + \frac{\partial (J\bar{H}_\alpha)}{\partial \xi_\alpha} = 0 \tag{1}$$

where repeated indices denote the summation over the three coordinate directions and an overbar indicates a grid-filtered quantity. The quantity $\bar{Q} = [\bar{\rho}, \bar{\rho}\bar{u}_\beta, \bar{\rho}\bar{e}]^T$ represents the vector of the conservative variables, i.e., the density, the momentum fluxes, and the specific energy, $J = |\partial(\xi_\alpha)/\partial(x_\beta)|$ is the metric Jacobian, and $\bar{H}_\alpha$ denotes the difference of the inviscid fluxes $\bar{F}_\alpha^I$ and the viscous fluxes $\bar{F}_\alpha^V$

$$\bar{H}_\alpha = \bar{F}_\alpha^I - \bar{F}_\alpha^V = \begin{pmatrix} \bar{\rho}\bar{U}_\alpha \\ \bar{\rho}\bar{u}_\beta\bar{U}_\alpha + \bar{p}\frac{\partial \xi_\alpha}{\partial x_\beta} \\ \bar{U}_\alpha(\bar{\rho}\bar{e} + \bar{p}) \end{pmatrix}$$
$$+ \frac{1}{Re}\begin{pmatrix} 0 \\ \frac{\partial \xi_\alpha}{\partial x_\varphi}\bar{\sigma}_{\beta\varphi} + Re\bar{\tau}_{\beta\varphi} \\ \frac{\partial \xi_\alpha}{\partial x_\varphi}(\bar{u}_\beta\bar{\sigma}_{\beta\varphi} + \bar{q}_\varphi + \bar{\Gamma}_\varphi) \end{pmatrix} \tag{2}$$

with $\bar{p}$ determined by the filtered state equation

$$\bar{p} = \frac{1}{\gamma}\bar{\rho}\bar{T} \quad . \tag{3}$$

The Stokes tensor $\bar{\sigma}_{\alpha\beta} = -2\mu(\bar{S}_{\alpha\beta} - \frac{1}{3}\bar{S}_{\varphi\varphi}\delta_{\alpha\beta})$ can be expressed via the filtered quantities

$$\bar{S}_{\alpha\beta} = \frac{1}{2}(\frac{\partial \bar{u}_\alpha}{\partial \xi_\varphi}\frac{\partial \xi_\varphi}{\partial x_\beta} + \frac{\partial \bar{u}_\beta}{\partial \xi_\varphi}\frac{\partial \xi_\varphi}{\partial x_\alpha}) \quad . \tag{4}$$

The fine-scale stresses $\bar{\tau}_{\alpha\beta}$ and the energy flux $\bar{\Gamma}_\alpha$ generated by the convective terms can be formulated using the subgrid scale model. The quantities $\bar{U}_\alpha$ and $\bar{q}_\beta$ represent the contravariant velocity $\bar{U}_\alpha = \bar{u}_\beta\partial\xi_\alpha/\partial x_\beta$ and Fourier's heat flux

$$\bar{q}_\beta = -\frac{k}{Pr(\gamma - 1)}\frac{\partial \bar{T}}{\partial x_\beta} \quad , \tag{5}$$

2

where $\bar{T}$ is the temperature and γ the ratio of specific heats. The Reynolds and the Prandtl number are defined by $Re = \rho_\infty u_\infty L/\mu_\infty$ and $Pr = \mu_\infty c_p/k_\infty$. The molecular viscosity is evaluated using $\mu = \bar{T}^{0.72}$. Assuming a constant Prandtl number the relation $k(\bar{T}) = \mu(\bar{T})$ holds for the thermal conductivity.

NUMERICAL METHOD

Although it is generally accepted that a difference scheme of at least second-order accuracy is sufficient to perform LES, it is crucial to minimize the amount of numerical dissipation of the scheme. The turbulent flow is characterized by strong interactions between various scales of motion. Schemes with a large amount of artificial viscosity significantly impair the level of energy distribution governed by the small-scale structures and therefore distort the physical representation of the dynamics of small as well as large eddies. It has been shown that a mixed central-upwind AUSM (advective upstream splitting method) scheme with low numerical dissipation could remedy this problem (Meinke et al., 2002), which is why a second-order accurate method is used in this study.

The AUSM method was introduced by Liou and Steffen (1993) who split the inviscid fluxes into a convective and a pressure term and reformulated the convective expression by inserting the local sound velocity c. Dropping the overbars this leads to

$$F_\alpha^I = F_\alpha^c + F_\alpha^p$$
$$= \frac{U_\alpha}{c} \underbrace{\begin{pmatrix} \rho c \\ \rho c u_\beta \\ \rho c(e + \frac{p}{\rho}) \end{pmatrix}}_{f_\alpha^c} + \begin{pmatrix} 0 \\ p\frac{\partial \xi_\alpha}{\partial x_\beta} \\ 0 \end{pmatrix} \quad . \quad (6)$$

The numerical flux F_α^c on the cell face, e.g. $i \pm \frac{1}{2}, j, k$, reads

$$F_\alpha^c = \frac{1}{2}\Big[\frac{Ma_\alpha^+ + Ma_\alpha^-}{2}(f_\alpha^{c+} + f_\alpha^{c-})$$
$$+ \frac{|Ma_\alpha^+ + Ma_\alpha^-|}{2}(f_\alpha^{c+} - f_\alpha^{c-})\Big]_{i\pm\frac{1}{2},j,k} \quad (7)$$

where the fluxes $f_\alpha^{c\pm}$ and the Mach numbers $Ma_\alpha^\pm$ are determined by left and right interpolated variables obtained using a MUSCL (monotonic upstream centered schemes for conservation laws) approach for the primitive variables.

The remaining pressure term can be formulated by

$$p^\pm = p^\pm(\frac{1}{2} \pm \chi Ma_\alpha^\pm) \quad . \quad (8)$$

The parameter χ, that represents the rate of change of the pressure ratio with respect to the local Mach number, determines the numerical dissipation of the scheme. A central splitting with clearly less numerical dissipation is obtained at $\chi = 0$.

The discretization of the friction and heat conduction expressions plays a less important role in turbulent flow than that of the nonlinear inviscid terms. The viscous terms are approximated by second-order accurate central differences. An explicit five-step Runge-Kutta time stepping scheme is used for the temporal integration. Using the Runge-Kutta coefficients $\alpha_l = (\frac{1}{4}, \frac{1}{6}, \frac{3}{8}, \frac{1}{2}, 1)$ a method of second-order accuracy in time with a maximum Courant number of 4 for central schemes results.

FLOW CONFIGURATION

The flow model for the simulation is shown in figure 1. In the near future some experimental results using the particle image velocimetry (PIV) technique will be available for the same configuration. The origin of the frame of reference coincides with the plate surface and the center of the hole. The coordinates x, y, z represent the streamwise, normal, and spanwise direction. The flow parameters and the geometrical parameters are summarized in table 1.

Table 1: Flow and Geometry Parameters

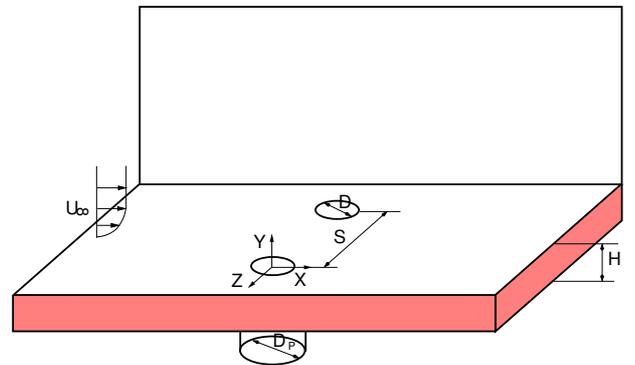| Re_∞	Ma	R	D	$\frac{\delta}{D}$	$\frac{S}{D}$	$\frac{H}{D}$
400,000	0.2	0.1	1	2	3	12

Fig.1: Schematic of the Flow Configuration

To mimic the flow parameters in a gas turbine a turbulent flat plate boundary layer at a local Reynolds number of $Re_\infty = 400,000$ interacts with a jet, which is part of a complete row of jets that are located perpendicular to the streamwise direction of the boundary layer flow. The ratio of the local boundary layer thickness to the hole diameter is $\frac{\delta}{D} = 2$. The velocity ratio $R = 0.1$ is rather small, it is, however, a typical value when film cooling for gas turbine blades is considered. The whole integration domain comprises a plenum under the jet hole, a pipe connecting the plate and the plenum, and the region where the boundary layer interacts with the jet. Since the plenum is part of the computational domain no empirical information such as the discharge coefficient has to be prescribed. The flow rate and the velocity distribution at the jet exit are determined in the computation.

BOUNDARY CONDITIONS

In the simulation of turbulent boundary layers the problem of how to prescribe time-dependent turbulent inflow conditions at the upstream boundary is encountered. In general, the flow downstream of the entrance

3

boundary is highly dependent on the conditions at the inlet, making it necessary to specify a realistic time series of turbulent fluctuations that are in equilibrium with the mean flow. This requirement dictates the inflow data to satisfy the Navier-Stokes equations, which in turn implies that an independent simulation is to be used to generate the inflow distribution. The formulation of the inflow boundary condition for the jet in a crossflow calculation is based on a slicing technique. That is, the flow variables at the entrance of the domain are obtained from a simultaneously conducted LES of a spatially developing turbulent boundary layer flow, as shown in figure 2, such that the level of turbulence intensity is physically correct. To implement the auxiliary turbulent boundary layer simulation where an inflow boundary condition is also needed a rescaling technique for compressible flow is applied.

turbulent boundary layer domain

Fig.2: Sketch of Rescaling and Slicing Methods

The rescaling method is a means of determining the properties at the inlet plane based on the solution downstream (Lund et al., 1998). In other words, the flow field extracted from a plane near the domain exit is rescaled by some appropriate laws and reintroduced as a boundary condition at the inlet. In effect, this procedure results in a straightforward spatially evolving simulation that generates its own inflow data. The general rescaling process is concisely described in the following.

To implement the rescaling method, first decompose the velocity into a mean and a fluctuating part. For example, the decomposition of the instantaneous streamwise velocity $\bar{u}$ is achieved by defining the mean value U as an average in the spanwise direction and in time. Then, the velocity fluctuation u' is defined as

$$u'(x,y,z,t) = \bar{u}(x,y,z,t) - U(x,y) \quad . \tag{9}$$

Applying the law of the wall in the inner region and

the defect law in the outer region, the mean flow at the downstream station (indicated by subscript re) can be linked with that at the inlet (indicated by subscript in) via the following equations

$$U_{in}^{inner} = \psi U_{re}(y_{in}^+) \tag{10}$$

$$U_{in}^{outer} = \psi U_{re}(\eta_{in}) + (1-\psi)U_\infty \tag{11}$$

where $y^+ = (u_\tau y)/\nu$ is the wall coordinate, $u_\tau = \sqrt{\nu(\partial u/\partial y)_{wall}}$ is the friction velocity, $\eta = y/\delta$ is the outer coordinate, and U_∞ is the free-stream velocity. A similar formulation is chosen for the velocity fluctuations

$$(u')_{in}^{inner} = \psi(u')_{re}(y_{in}^+, z, t) \tag{12}$$
$$(u')_{in}^{outer} = \psi(u')_{re}(\eta_{in}, z, t) \tag{13}$$

where the rescaling factor ψ is defined as

$$\psi = \frac{u_{\tau,in}}{u_{\tau,re}} \quad . \tag{14}$$

Equations (10) - (14) provide a means of rescaling the mean and fluctuating velocity for the inner and outer regions of the boundary layer.

The extension of the rescaling method to compressible flow can be found in the paper (El-Askary et al., 2001). Introducing the Walz equation (1969) the mean static temperature T follows

$$\frac{T}{T_\infty} = 1 + A(1 - \frac{U^2}{U_\infty^2}) \tag{15}$$

where $A = 0.5(\gamma - 1)rMa^2$, r is the recovery factor determined by $r = Pr^{1/3}$, and Ma is the free-stream Mach number. Following Bradshaw (1977) we introduce the static temperature fluctuation T'

$$\frac{T'(y,z,t)}{T} = -(\gamma - 1)M^2 \frac{u'(y,z,t)}{\bar{u}(y,z,t)} \tag{16}$$

where M is the local Mach number. Imitating the velocity rescaling process the mean static temperature T and its fluctuation T' can be rescaled using the following equations

$$T_{in}^{inner} = \psi^2 T_{re}(y_{in}^+) + C_1 T_\infty \tag{17}$$

$$T_{in}^{outer} = \psi^2 T_{re}(\eta_{in}) - C_2 \frac{U_{re}(\eta_{in})}{U_\infty} T_\infty + C_3 T_\infty \tag{18}$$

$$(T')_{in}^{inner} = \psi^2 (T')_{re}(y_{in}^+, z, t) \tag{19}$$

$$(T')_{in}^{outer} = \psi^2 (T')_{re}(\eta_{in}, z, t) - C_2 \frac{(u')_{re}(\eta_{in}, z, t)}{U_\infty} T_\infty \tag{20}$$

with $C_1 = (1+A)(1-\psi^2)$, $C_2 = 2A\psi(1-\psi)$, $C_3 = (1-\psi)(1+\psi+2A\psi)$.

On the wall the non-slip condition holds and an adiabatic surface is assumed

$$\bar{u}_\beta = 0 \tag{21}$$

$$\frac{\partial \bar{T}}{\partial n} = 0 \quad , \tag{22}$$

4

where n is the direction normal to the wall. In the spanwise direction full periodic boundary conditions are imposed. The stagnation pressure value is specified at the inlet of the plenum (Fig. 2) where the jet flow is driven by the pressure difference between the plenum and the crossflow. At the outer circumferential surface of the plenum the mass flux is assumed to vanish asymptotically. A characteristic approach is applied at the outflow boundaries. To damp the numerical reflections introduced by the outflow boundary conditions a sponge layer zone is used, as shown in figure 2, in which source terms are added to the right-hand side of the governing equations. The source terms are computed as a function of the deviation of the instantaneous solution $\bar{Q}$ from the analytical distribution Q_a based on the logarithmic law

$$S = \sigma(\bar{Q}(t,\vec{x}) - Q_a(\vec{x})) \quad . \qquad (23)$$

The parameter σ is a function of the distance from the boundaries and decreases from σ_{max} to 0 within the sponge layer zone. The value for σ_{max} is chosen to be 0.5, which was determined in test simulations under the condition to minimize numerical reflections.

RESULTS AND DISCUSSION

To validate the numerical method described above a turbulent boundary layer over a flat plate is calculated at $Ma = 0.4$ and $Re_{\delta_0} = 14400$ ($Re_{\theta_0} = 1400$), where Re_{δ_0} and Re_{θ_0} are the Reynolds numbers based on the boundary layer thickness δ_0 and momentum thickness θ_0 at the inlet, respectively. Two different grids are used to study the effect of grid resolution, i.e., a relatively coarse grid with $361 \times 113 \times 17$ grid points and a finer grid with $721 \times 113 \times 33$ grid points in a computational domain of $30\delta_0 \times 3.5\delta_0 \times 0.64\delta_0$ in the streamwise, wall normal, and spanwise direction. In wall units (using the wall shear evaluated at the inlet) the first mesh resolution normal to the wall is $\Delta y^+ = 1.0$ for both cases.

In figure 3 the mean streamwise velocity profiles in inner-law scaling obtained with different outflow boundary conditions and grid resolutions are compared with the logarithmic law, which consists of the viscous sublayer $y^+ \leq 5.0, u/u_\tau = y^+$, the buffer layer $5.0 < y^+ \leq 30.0, u/u_\tau = 5.0 \ln y^+ - 3.05$, and the logarithmic layer $y^+ > 30.0, u/u_\tau = 2.5 \ln y^+ + 5.5$. The solution in the case of the coarse grid without the sponge layer demonstrates the influence of the formulation of the exit boundary condition. All profiles closely match the analytical solution and the fine grid yields the best agreement.

The turbulence intensities at the position of $Re_\theta = 1850$ of the fine grid LES are compared with data from (Lund et al., 1998) in figure 4. All distributions evidence a good agreement with the findings from the literature such that it can be stated that reliable inflow data are provided by the flat plate LES. Since the similar spanwise and normal resolutions are used for the jet in a crossflow (JICF) problem, it is fair to conclude that the major turbulent structures also are captured in the interacting flow field.

We turn now to the analysis of the JICF problem. The inflow boundary is located $8D$ upstream of the jet
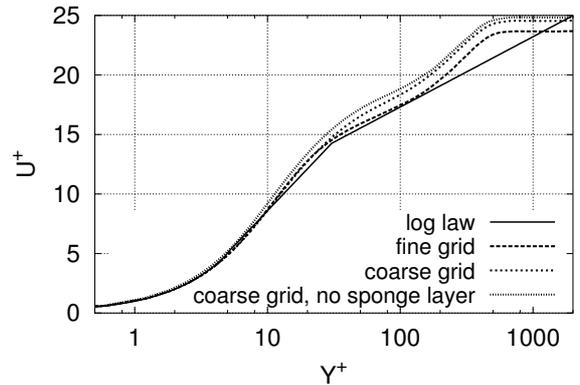

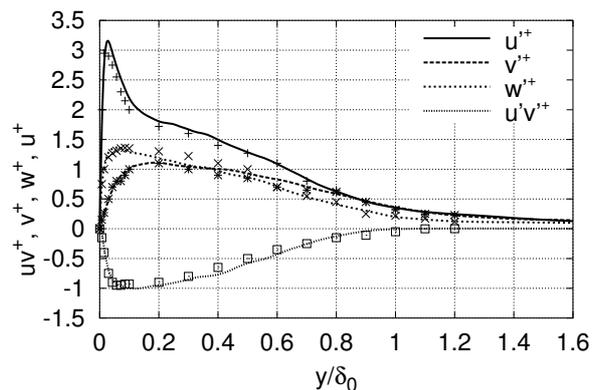Fig.3: Mean Streamwise Velocity Distributions

Fig.4: Reynolds Stress Components Compared with Data from Lund et al. (1998) (Symbols)

hole center such that the influence of the jet flow on the upstream flow field can be neglected, i.e., the inflow LES is independent from the JICF LES. The grid lines at the inlet area coincide with those of the boundary layer simulation, i.e., no interpolation of the solution is required. Various parts of the computational grid of the jet in a crossflow problem are shown in figure 5. The total mesh consists of 4.6 millions grid points distributed in 32 blocks, 5 of which are used for the turbulent boundary layer over the flat plate simulation. The grid points are clustered near the solid surfaces. The first control volume next to the flat plate has the dimension of $\Delta y = 0.004D$, which corresponds to $\Delta y^+ = 1.0$ scaled by the friction velocity of the incoming turbulent boundary layer. In the streamwise and spanwise directions roughly 369×65 grid points are used to discretize the domain of $35D \times 3D$.

As in other turbulent flows, the coherent structures dominate the behavior of the jet in a crossflow. Advances in experimental flow visualization techniques have provided the means for researchers to probe the flow and identify the large-scale features. Fric & Roshko (1994) categorize the coherent structures in the flow field into four groups: the horseshoe-like vortex wrapped around the exit jet column, the ring vortices contained in the jet shear layer, the wake structure formed down-
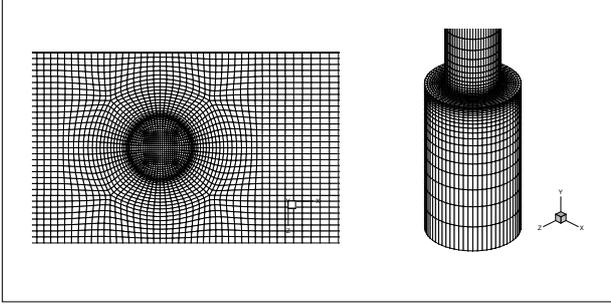
Fig.5: Grids of JICF, Top View of the Jet Exit Region (Left) and Plenum (Right), Every 2nd Grid Point Is Shown

stream of the jet exit, and a counter-rotating vortex pair (CVP), which is formed as the jet transitions into the crossflow direction. All of these structures are observed in the LES. To better understand the formation of the structures described by Fric & Roshko (1994), first some instantaneous solutions are visualized using streamlines and the λ_2-criterion (Jeong and Hussain, 1995). Subsequently, the time-averaged flow field is presented.

The temporal evolution of the streamlines in the central plane near the jet exit is presented in figure 6. Here one time unit corresponds to $u_\infty \Delta t / D = 1$. Compared to the experimental investigations for $R = 0.5$ in (Foss, 1980) and (Andreopoulos and Rodi, 1984) the qualitative agreement on the main flow structures is achieved. Due to the interaction of the crossflow and the jet flow the crossflow in the exit region behaves as if a flap covers a little part of the jet exit. The rather large crossflow velocity compared to the jet velocity causes the jet streamlines to form a vortex in the pipe. The crossflow is only slightly deflected by the exhausting jet. The separation of the oncoming boundary layer is indicated by the vortex just at the edge of the exit. This can be deemed the origin of the horseshoe-like vortex. Some pipe fluid is entrained into this vortex as indicated in figure 6. The local high pressure area caused by the stagnation effect of the jet flow initiates a precessing vortex in the pipe. On the leeside of the jet exit the wake region with a complex three-dimensional flow pattern develops and the flow structures vary intensely with time. Since the velocity ratio investigated in the literatures is much higher than the presented computational analysis and the accuracy of the measurements near to the wall is poor, no comparison about the extent of the separation region downstream of the jet exit is made.

The λ_2-criterion, which is used to visualize the vortical structures, is based on the decomposition of the velocity gradient tensor into a symmetric and an asymmetric part

$$\nabla \vec{u} = \begin{pmatrix} \bar{u}_x & \bar{u}_y & \bar{u}_z \\ \bar{v}_x & \bar{v}_y & \bar{v}_z \\ \bar{w}_x & \bar{w}_y & \bar{w}_z \end{pmatrix} = \overline{\overline{S}} + \overline{\overline{\Omega}} \quad , \quad (24)$$
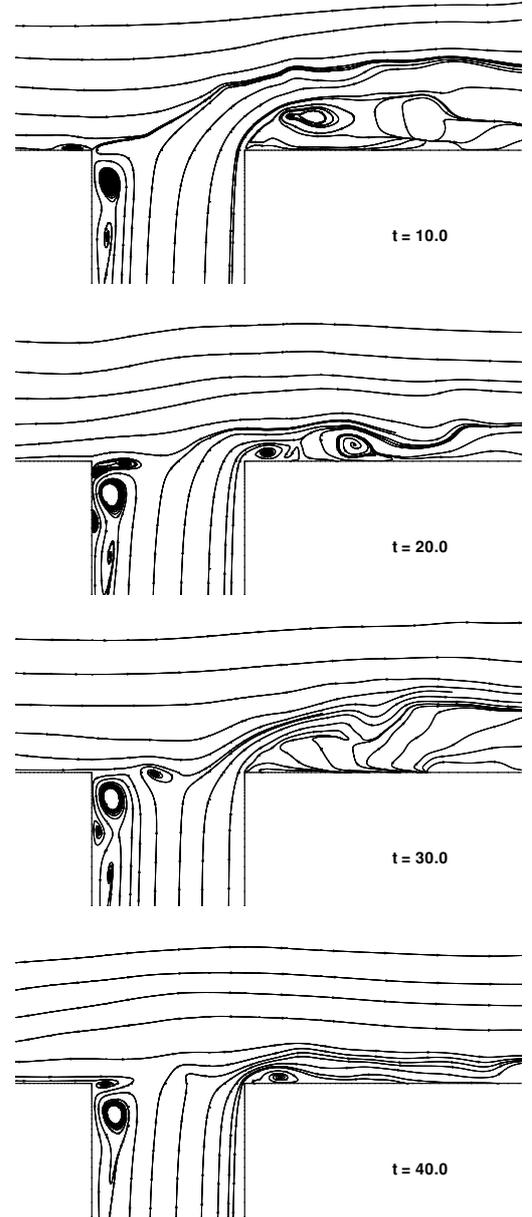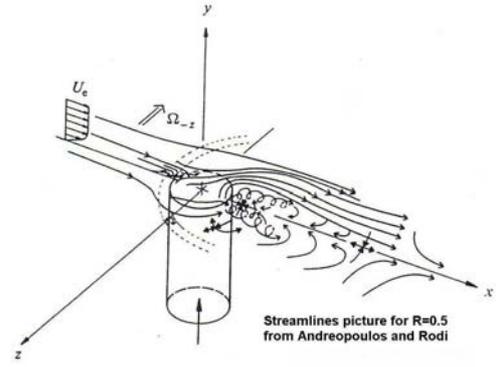
Fig.6: Temporal Evolution of the Streamlines in the Central Plane Near the Jet Exit at $R = 0.1$

where

$$\overline{\overline{S}} = \frac{1}{2} \begin{pmatrix} 2\bar{u}_x & \bar{u}_y + \bar{v}_x & \bar{u}_z + \bar{w}_x \\ \bar{v}_x + \bar{u}_y & 2\bar{v}_y & \bar{v}_z + \bar{w}_y \\ \bar{w}_x + \bar{u}_z & \bar{w}_y + \bar{v}_z & 2\bar{w}_z \end{pmatrix} \quad (25)$$

6

and

$$\overline{\overline{\Omega}} = \frac{1}{2} \begin{pmatrix} 0 & \bar{u}_y - \bar{v}_x & \bar{u}_z - \bar{w}_x \\ \bar{v}_x - \bar{u}_y & 0 & \bar{v}_z - \bar{w}_y \\ \bar{w}_x - \bar{u}_z & \bar{w}_y - \bar{v}_z & 0 \end{pmatrix} \quad . \quad (26)$$

Jeong & Hussain found that the second negative eigenvalue of the symmetric matrix

$$\overline{\overline{M}} = \overline{\overline{S}}^2 + \overline{\overline{\Omega}}^2 \qquad (27)$$

corresponds to a local pressure minimum and closed streamline pattern. Both properties are also characteristic for a vortex pattern. In figure 7 the vortex structures near the jet exit for an instantaneous solution are visualized using the λ_2-criterion. The turbulence characteristics within the boundary layer are clearly visible. Due to the ratio $R = 0.1$ the jet flow possesses only a slight impact on the vortical pattern which is indicated by the somewhat bulkier vortex structure just downstream of the jet exit.
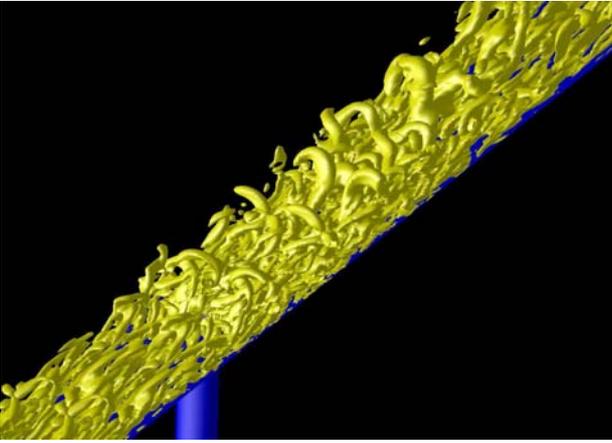
Fig.7: λ_2-Contours Near the Jet Exit at $R = 0.1$

Some pronounced features in the flow can be clarified by averaging the instantaneous solutions over a long period of time. In the following, the pictures are plotted for the mean flow field averaged over a non-dimensional time of $\Delta t = 50$. In figure 8 the wall streamlines are depicted in the wake region of the jet exit. In this region the streamwise velocity of the crossflow accelerates and the conservation of mass requires fluid to move towards the plane of the symmetry. Very close to the wall a reverse flow region forms. Fluid from the cross stream is entrained into this region, travels upstream, and is lifted upwards by the jet flow and washed downstream in the shear layer formed by the jet and the crossflow.

The development of the counter-rotating vortex pair (CVP) at different streamwise locations downstream of the jet exit is shown in figure 9. The CVP occurs in the center of the plane. On each side of the CVP an additional vortex located closer to the wall exists. These counter rotating vortices belong to the horseshoe-like vortex. When moving downstream the strength of the CVP reaches a maximum value before it decays in the wake far away from the jet exit. The asymmetry of the
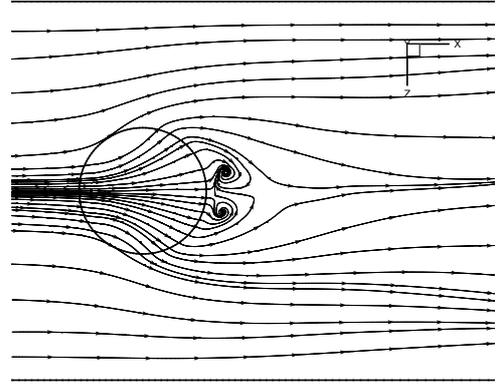
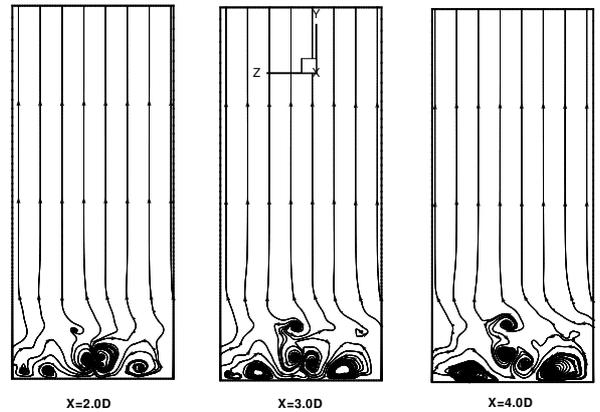Fig.8: Streamlines of the Mean Flow Field in the Wake Region of the Jet

Fig.9: Development of a Counter-Rotating Vortex Pair at Different Streamwise Locations

results indicates that the averaging time is still to be extended.

The size of the separation area downstream of the jet exit is visualized in figure 10 using the $Ma = 0.02$ isosurface and the local vector field in the symmetry plane. Due to the small jet velocity the recirculation area extends in the streamwise direction only $1.3D$. The existence of the separation zone prevents the cooling jet fluid to cover effectively the wall surface just downstream of the jet exit. Furthermore, the hot gas stream is entrained underneath the coolant and lifts the coolant further away from the wall. Both interacting effects decrease the cooling efficiency.

CONCLUSION

Large-eddy simulations (LES) of the jet in a crossflow problem have been carried out to investigate in detail the intricate vortex structures in the flow field. The parameters used in the calculation correspond to those encountered in film cooling of turbine blades. To provide realistic time-dependent flow properties at the inlet boundary an LES of a spatially developing turbu-
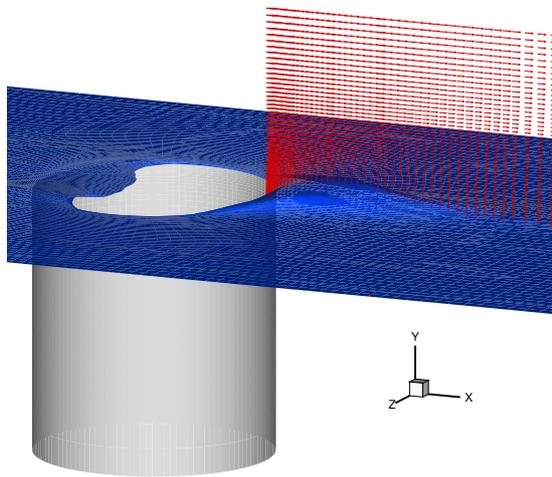
Fig.10: Visualization of the Separation Region

lent boundary layer is computed simultaneously using a rescaling method for compressible flat plate flow. The comparison between the results of a turbulent boundary layer over a flat plate simulation and data from the literature validates the application of the LES. The main JICF flow structures are analyzed by visualizing the instantaneous and the time-averaged flow field. The separation area downstream of the jet exit decreases the cooling efficiency.

ACKNOWLEDGMENTS

References

Andreopoulos, J., and Rodi, W., 1984, "Experimental Investigation of Jets in a Crossflow," *Journal of Fluid Mechanics*, Vol. 138, pp.93-127.

Bohn, D. E., Becker, V., Kusterer, K., Ardey, S., and Fottner, L., 1997, "The Influence of Slot Injection and Shower-Head Injection on the 3D Flow Field of a Film-Cooled Turbine Blade under Consideration of Side-Wall Effects," *AIAA Paper*, No.97/7162 .

Bradshaw, P., 1977, "Compressible Turbulent Shear Layers," *Annual Review of Fluid Mechanics*, Vol. 9, pp.33-54.

Chernobrovkin, A., and Lakshminarayana, B., 1999 "Numerical Simulation and Aerothermal Physics of Leading Edge Film Cooling," *Journal of Power and Energy*, Vol. 213, pp.103-118.

El-Askary, W. A., Meinke, M., and Schröder, W., 2001, "Towards the Numerical Analysis of Trailing-Edge Noise," *Deutscher Luft- und Raumfahrtkongress 2001*, Hamburg.

Foss, J., 1980, "Interaction Region Phenomena for the Jet in a Cross-flow Problem," *Rep.* SFB 80/E/161, *Univ. Karlsruhe.*

Fric, T. F., and Roshko, A., 1994, "Vortical Structure in the Wake of a Transverse Jet," *Journal of Fluid Mechanics*, Vol. 279, pp.1-47.

Garg, V. K., and Ameri, A. A., 1997, "Comparison of Two-Equation Turbulence Models for Prediction of Heat Transfer on Film-Cooled Turbine Blades," *Numerical Heat Transfer*, Vol. 31, pp.347-371.

Gartshore, I., Salcudean, M., and Hassan, I., 2001, "Film Cooling Injection Hole Geometry: Hole Shape Comparison for Compound Cooling Orientation," *AIAA Journal*, Vol. 39, pp.1493-1499.

Jeong, J., and Hussain, F., 1995, "On the Identification of a Vortex," *Journal of Fluid Mechanics*, Vol. 285, pp.69-94.

Liou, M. S., and Steffen, C. J., 1993, "A New Flux Splitting Scheme," *Journal of Computational Physics*, Vol. 107, pp.23-39.

Lund, T. S., Wu, X., and Squires, K. D., 1998, "Generation of Turbulent Inflow Data for Spatially-Developing Boundary Layer Simulations," *Journal of Computational Physics*, Vol. 140, pp.233-258.

Meinke, M., Schröder, W., Krause, E., and Rister, T., 2002, "A Comparison of Second- and Sixth-Order Methods for Large-Eddy Simulations," *Computers & Fluids*, Vol. 31, pp.695-718.

Rogallo, R. S., and Moin, P., 1984, "Numerical Simulation of Turbulent Flows," *Annual Review of Fluid Mechanics*, Vol. 16, pp.99-137.

Walz, A., 1969, "Boundary Layers of Flow and Temperature," MIT Press.